Lab on a Chip

PAPER

Cite this: DOI: 10.1039/c6lc01309k

High efficiency hydrodynamic bacterial electrotransformation†

Paulo A. Garcia,‡[a] Zhifei Ge,‡[a] Laura E. Kelley,[b] Steven J. Holcomb[a] and Cullen R. Buie*[a]

Received 21st October 2016,
Accepted 6th December 2016

DOI: 10.1039/c6lc01309k

www.rsc.org/loc

Synthetic biology holds great potential for addressing pressing challenges for mankind and our planet. One technical challenge in tapping into the full potential of synthetic biology is the low efficiency and low throughput of genetic transformation for many types of cells. In this paper, we discuss a novel microfluidic system for improving bacterial electrotransformation efficiency and throughput. Our microfluidic system is comprised of non-uniform constrictions in microchannels to facilitate high electric fields with relatively small applied voltages to induce electroporation. Additionally, the microfluidic device has regions of low electric field to assist in electrophoretic transport of nucleic acids into the cells. The device features hydrodynamically controlled electric fields that allow cells to experience a time dependent electric field that is otherwise difficult to achieve using standard electronics. Results suggest that transformation efficiency can be increased by ~4×, while throughput can increase by 100–1000× compared to traditional electroporation cuvettes. This work will enable high-throughput and high efficiency genetic transformation of microbes, facilitating accelerated development of genetically engineered organisms.

Introduction

Genetic transformation of bacteria for synthetic biology

Genetic engineering and synthetic biology hold great potential to develop microbiome therapeutics,[1] artificial photosynthesis,[2] biomolecular manufacturing,[3] *in vivo* diagnostics,[4] and targeted cancer treatments.[5] A key step in genetic engineering is delivering genetic materials into cells. However, there is no single technology that solves all problems in intracellular delivery of genetic materials. Delivery of genetic material through viral vectors, for example, is very efficient in both bacterial[6] and mammalian cells,[7] but this procedure is cell-type specific, and has problems with immunogenicity and random insertion when moving into clinical applications.[8] Cell squeezing is a new invention in intracellular delivery of large molecules, but is currently limited to mammalian cells.[12,13] Conjugation is widely used among transformations of *E. coli*,[9] *Mycobacteria*,[10] and *Bacillus*,[11] but has problems with cell-type specificity and is not scalable to other bacterial species.[11]

Since its invention in the 1980s,[14] electroporation (EP) has been widely used for introducing genetic materials into both mammalian[15] and bacterial cells.[15] Additionally, delivery of very large size plasmids, such as bacterial artificial chromosomes (BAC, typically 150–350 kbp) can be achieved.[16] Electroporation is not species specific, but without optimization, electroporation can lead to high cell mortality, high experimental cost, low transformation efficiency, and low throughput. The low efficiency can result from cell properties (such as thick cell walls), plasmid size, and the physical and chemical conditions of the transformation process.[17,18,54] Electroporation uses pulsed electric fields to reversibly disrupt the cell envelope for intracellular delivery of exogenous materials, such as DNA.[14,18,27] This method is strongly dependent on the electric field strength experienced by the cells: fields that are too high cause irreversible electroporation and cell lysis causing death.[19] While lysis has many important applications such as non-thermally treating inoperable tumors, it hinders genetic engineering.[20–23] Conversely, electric fields that are too low are insufficient to introduce exogenous materials and cells cannot be engineered. As a result, the field strength has to be closely monitored and tailored to each cell type for electroporation to achieve optimal levels of viability

[a] *Department of Mechanical Engineering, Massachusetts Institute of Technology, 77 Massachusetts Ave, Cambridge, MA, 02139, USA. E-mail: crb@mit.edu*
[b] *Department of Biological Engineering, Massachusetts Institute of Technology, 77 Massachusetts Ave, Cambridge, MA, 02139, USA*

† Electronic supplementary information (ESI) available. See DOI: 10.1039/c6lc01309k

‡ These authors contributed equally to this work.

and transformation efficiency.[24–26] This paper focuses on increasing bacterial genetic transformation throughput and efficiency *via* improved design of electroporation systems using microfluidics.

Microfluidic electroporation for mammalian cell transfection

Microfluidic electroporation for mammalian cell applications has demonstrated significantly improved transfection efficiency and higher cell viability compared to cuvette-based electroporation.[27–29] Flow-through transfections in microfluidic devices generally use a fraction of the experimental sample and lower voltages than cuvette-based electroporation, which helps to maintain high cell viability and high transfection efficiency.[27] A new type of transfection process involves immobilizing cells with channel constrictions that are smaller than the cell diameter. For example, microhole structures in silicon nitride dielectric membranes were used for initially trapping and subsequently electroporating single cells.[30] Similarly, nanochannels,[31,32] dielectrophoresis,[33] and magnetic tweezers[34] can be used to position cells prior to transfections with electroporation, enabling single-cell dosage control. With the ability to control single-cell dosage, the devices by L. Q. Chang and co-workers[33,34] are able to handle 40 000–60 000 cells per cm^2. Further advances have been realized by Khine *et al.* who developed a microfluidic chip that selectively immobilizes and electroporates single cells[35] while others developed 2D and 3D nanochannels to deliver transfection agents into mammalian cells with electroporation.[31,36] Kang *et al.* developed a microfluidic device for stem cell attachment, differentiation, and subsequent transfection of neurons on chip for studying cells in their natural state.[37] Another methodology for mammalian cell transfection uses flow-through processes in which groups of cells are exposed to sufficiently high electric fields when they flow-through particular regions of a microfluidic channel. Lu *et al.* pioneered microfluidic devices with a series of geometric constrictions with uniform cross-sectional areas for flow-through electroporation based on DC or AC signals.[38,39] Lu and co-workers further developed vortex-assisted microfluidic applications to improve transfection efficiency by increasing the fraction of the total membrane surface that is permeabilized.[40] Yun *et al.* demonstrated sequential delivery of different molecules with independent and precise dosage controllability into human cancer cells with inertial focusing.[41] Finally, Adamo *et al.* developed a flow-through microfluidic device with a comb electrode layout and successfully characterized HeLa cell transfection.[12]

Despite significant advances in microfluidic transfection of mammalian cells, transformation of bacteria requires several modifications to the techniques currently being used in mammalian cells. To transform bacteria, the devices need to be able to achieve electric fields that are approximately one order of magnitude larger than what is required for mammalian cell transfection, primarily because bacteria are much smaller in size (nominally around 1 μm). With these differences, significant Joule heating can occur within the device during pulse application as a result of the high electric fields required for bacterial transformation. The resulting temperature in the channel could be high enough to compromise cell viability. Finally, geometric constrictions to immobilize bacteria, as has been used with mammalian cells are unrealistic. To immobilize bacteria the constrictions need to be in the tens-to-hundreds of nano-meters in diameter, resulting in significantly higher fluidic resistance compared with microchannels used for mammalian cells. Furthermore, the dimensions are so small that they would be challenging to fabricate at large scale with current technologies. Despite these challenges, an appropriately modified microfluidic system has the potential to realize the same benefits for bacteria as have been demonstrated for several mammalian cell applications due to the potential for higher transformation efficiency, higher throughput, and higher viability when compared to traditional cuvette based electroporation approaches.[28]

Microfluidic flow-through EP for bacterial transformation

We have developed, to our knowledge, the first continuous flow system demonstrating bacterial transformation with electroporation. We estimate that our microfluidic approach could outperform the state of the art electroporation techniques, based on 100–1000× increase in throughput and 4× increase in transformation efficiency when compared to cuvette based electroporation approaches. In our microfluidic system, we have designed channels with non-uniform cross-sectional areas so that bacteria experience time dependent electric fields that would be difficult to achieve using standard electronics.[26] Additionally, the microfluidic device has regions of high and low electric field for inducing electroporation and subsequently performing electrophoretic-assisted delivery of nucleic acids into cells.[26,42] In essence, this system exploits local channel geometry to alter local electric field magnitude, providing a hydrodynamic scheme to manipulate the electric pulse seen by flowing bacterial cells. The continuous flow system presented further enables automated processing.

Materials & methods

Modelling electric field, fluid flow, and temperature distributions

We have developed a computational model to determine channel geometries and experimental conditions that result in increased throughput and increased transformation efficiency. The computational models coupled electric, hydrodynamic, and thermal responses in COMSOL Multiphysics v5.1 (Burlington, MA) for the bilateral, converging, diverging, and straight constriction geometries studied. The goal is to operate with experimental conditions that are favorable for bacterial transformation without significantly compromising cell viability due to extremely high electric fields or exposure to lethal temperatures. Specifically, the electric field

distribution within the microfluidic devices is computed by solving the Laplace equation:

$$-\nabla\cdot(\sigma\nabla\varphi) = 0 \quad (1)$$

where σ is the electric conductivity of the electroporation buffer and φ the electric potential (Table 1). An electric conductivity of 0.002 S m^{-1} is measured for 10% (v/v) glycerol; however, it is assumed that the conductivity of the entire sample increased 5× in order to conservatively incorporate the increase in conductivity that occurs during electroporation.[43–45] The fluid flow is computed by solving 3D steady-state Navier–Stokes and continuity equations.[46] Additionally, the temperature distribution is determined by coupling the Joule heating term and fluid velocity distributions within the heat transfer in fluids module, using similar numerical techniques to those described by Gallo-Villanueva *et al.*[47] The following assumptions are made in the model: a) electrical insulation at every boundary except for the electrodes with $\varphi = V_0$ and $\varphi = 0$, b) specific flow rates at the inlet and no pressure at the outlet, c) no-slip conditions at the channel walls, d) incompressible fluid, and e) thermal insulation on the channel walls.

Device design and working principle

To evaluate the effect of channel geometry on transformation efficiency, four unique designs are compared with traditional 2 mm electroporation cuvettes, as shown in Fig. 1. The first geometry is bilaterally converging (Fig. 1a) with a minimum channel width of 50 μm at the center of the constriction. A minimum channel width of 50 μm is assigned for both the converging and diverging constrictions to maintain consistency across the channel geometries (Fig. 1b). The straight microchannel (Fig. 1c) is 50 μm in width, with a constant cross-sectional area along its entire 3 mm length. All four microfluidic channel geometries were 100 μm in depth. Additionally, Fig. 1a–c shows the electric field distributions corresponding to the four constriction geometries that are evaluated experimentally for inducing genetic transformation of the electrocompetent *Escherichia coli* DH10β and *Escherichia coli* K12 wildtype (WT). We select *E. coli* DH10β for transformation because it has been widely used in molecular biology as a model organism. Additionally, we evaluate the transformation efficiency of *E. coli* K12 wildtype since it contains native restriction and modification systems for DNA methylation and degradation, making it more challenging to engineer.[48] From these numerical simulations at an applied

Table 1 Physical parameters used in numerical simulations

Symbol	Quantity	Value	Units	Ref.
σ	Electric conductivity	0.01	S m^{-1}	—
ρ	Density	1000	kg m^{-3}	47
μ	Dynamic viscosity	1×10^{-3}	Pa S	47
k	Thermal conductivity	0.58	W m^{-1} K^{-1}	47
c_p	Heat capacity	4184.4	J kg^{-1} K^{-1}	47
T_i	Initial temperature	294.15	K	—

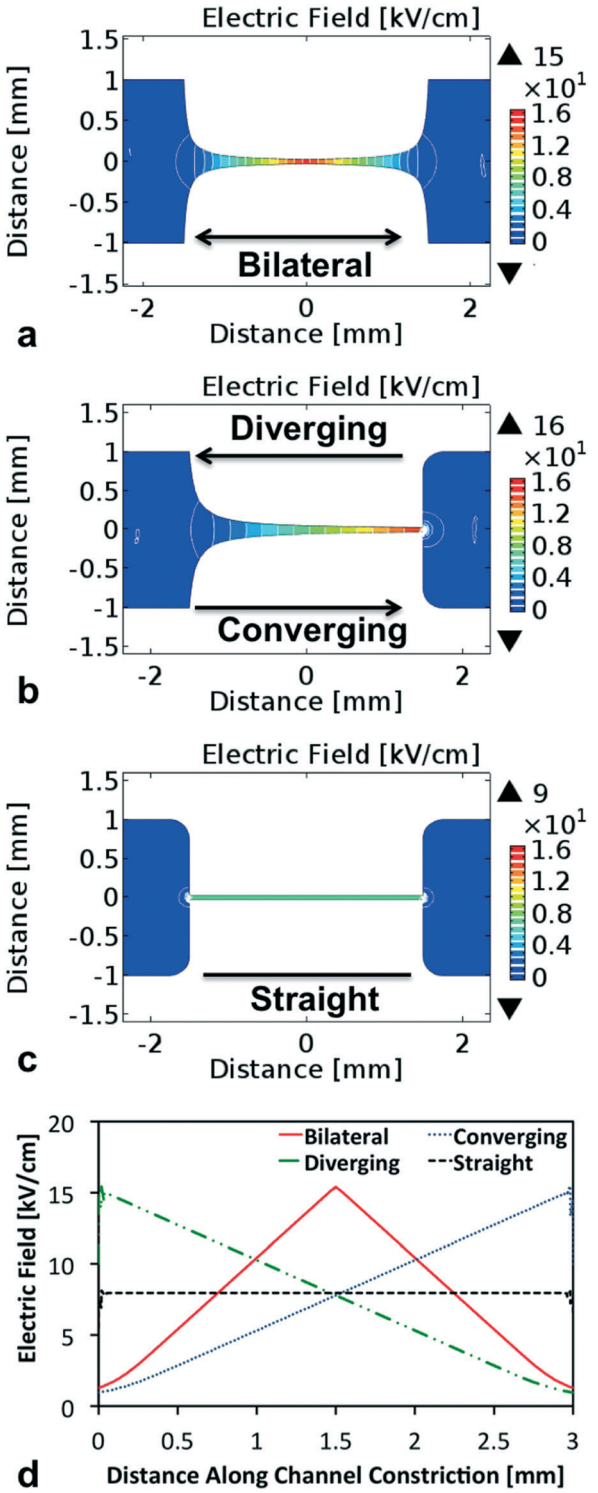

Fig. 1 Four designs of the microfluidic device depicting microchannels with a) a bilaterally converging constriction geometry, b) a diverging and converging constriction geometry depending on the flow direction (depicted by arrows), or c) a straight microchannel with uniform cross sectional area. Panel d shows the electric field strength in the microchannel along the centerline of the constriction region when a voltage of 2.5 kV is applied. Note: the non-uniform microchannels achieve ~2× higher E_{max} than the uniform microchannels.

voltage of 2.5 kV, it can be appreciated that the constrictions with non-uniform cross-sectional areas (E_{max} = 15–17 kV cm^{-1}) are able to amplify the electric field strength to magnitudes that are roughly two times higher than the microchannel with a uniform cross-sectional area (E_{max} = 9 kV cm^{-1}). The ability of the non-uniform designs to amplify the electric field more efficiently than straight channels is advantageous since it requires lower applied voltages to achieve the same maximum electric field. This translates into reduced deleterious effects resulting from the pulsed electric fields, such as excessive Joule heating or pH changes that could affect cell viability and prevent successful transformation. Fig. 1d plots the electric field along the centerline of each 3.0 mm constriction and further corroborates that a non-uniform geometry is advantageous to reach electric fields required for electroporation for a given applied voltage.

Test system setup for flow-through bacterial electroporation

Fig. 2 shows the overall test system setup. Cell suspensions (see Cell culture and preparation for electroporation) are driven by a syringe pump (Pump 11 Pico Plus Elite Syringe Pumps, Harvard Apparatus, Holliston, MA) at a particular flow rate for each experiment. Specifically, the samples in the straight channels were driven at 125 μL min^{-1} and the samples in the bilateral, converging, and diverging microchannels at 500 μL min^{-1}. The differences in flow rates ensure that the residence time within the constrictions is comparable due to the 4× volume difference between the non-uniform and uniform constriction geometries. Additional experiments are performed in the bilateral (250–4000 μL min^{-1}) and straight (62.5–1000 μL min^{-1}) microchannels to evaluate the influence of flow rate on transformation efficiency. The syringe pump, microchannel, and recovery media contained in Eppendorf tubes are connected with PVC tubing (ID 1/16 inch, OD1/8 inch, Tygon Tubing, McMaster Carr, Elmhurst, IL). The cell suspensions are driven through the microchannel and into recovery media. The electric field is applied from a function generator (Agilent 33220A, Agilent Technologies Inc., Lexington, MA) to the microchannel with a pair of 16-gauge stainless-steel dispensing needle electrodes. Signals from the function generator are amplified about 1000× by a high voltage power amplifier (TREK Model 623B high-voltage power amplifier, Trek Inc., Lockport, NY). The amplified electric signal is verified by an oscilloscope (DSO-X 2022A, Agilent Technologies Inc., Lexington, MA) through a high-voltage differential probe (Keysight N2891A, Keysight Technologies, Santa Rosa, CA) connected in parallel to the electrodes.

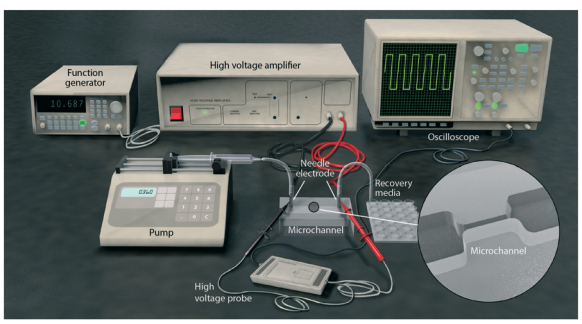

Fig. 2 Schematic of the test system setup. The programmable syringe pump drives the cell suspension through the microchannel and into the recovery media. The electric field is established in the microchannel by two dispensing needle electrodes, powered by the amplified voltage signal from the function generator.

Microfabrication protocol of devices

The photomasks are designed in AutoCAD 2014 (Autodesk, San Rafael, CA) with geometries as in Fig. 1 and printed by Fine-Line Imaging, Inc. (Colorado Springs, CO). The microchannels are fabricated using standard soft lithography techniques described previously by Garcia *et al.*[26] SU-8 (SU-8 2050, Micro-Chem, Westborough, MA) molds are patterned on silicon wafer using photolithography. After photolithography, the surfaces of the SU-8 master molds are treated under vacuum for 2 hours with tridecafluoro-1,1,2,2-tetrahydrooctyl-1-trichlorosilane (Sigma Aldrich, St. Louis, MO) before being used for molding. Next, the SU-8 masters are used to mold polydimethylsiloxane (PDMS) using Sylgard 184 (Dow Corning, Midland, MI) at a 10 : 1 ratio after 2 hour vacuum for air bubble removal. The PDMS devices are bonded to a glass slide after a 45 second plasma treatment and placed in an oven at 75 °C overnight before subsequent experiments.

Cell culture and preparation for electroporation

E. coli DH10β (New England Biolabs, Ipswich, MA) and *E. coli* K12 wildtype (Yale Coli Genetic Storage Center, CGSC 4404) are cultured overnight in a 3 mL test tube of Luria Broth (LB) medium. The following morning, 333 μL of cell culture is transferred to 100 mL of fresh growth media and allowed to grow to exponential phase before electroporation (OD_{600} ~ 0.5). Then, cell suspensions are concentrated 20× *via* centrifugation at 3500 rpm at 4 °C for 5 min (F0650 rotor, Allegra 64R Benchtop Centrifuge, Beckman Coulter, Indianapolis IN). During the concentration step, the supernatant is discarded and the cells are washed three additional times with pre-chilled to 4 °C 10% (v/v) glycerol and centrifugated at 8000 rpm for 5 min each time (F1202 rotor, Allegra 64R Benchtop Centrifuge, Beckman Coulter, Indianapolis IN). Cell concentration is confirmed *via* spectrophotometer measurement of OD_{600} = 0.5 at a 1 : 20 dilution ratio. Immediately prior to the electric pulsing, ampicillin resistance and green fluorescent protein (GFP) encoding DNA plasmids (Parts Registry K176011) are added to the cell solution for a final concentration of 1.0 ng μL^{-1}. Plasmid DNA is extracted using a QIAgen spin miniprep kit (QIAgen, Hilden, Germany).

Cell electroporation using microchannels or cuvettes

For cell electroporation in the microchannels, three independent cell samples of 100 μL with 1.0 ng μL^{-1} DNA plasmids are suctioned into the tygon tubing. Square wave pulses with

5 ms ON and 250 μs OFF cycles (95% duty cycle) are applied to the microchannel through the dispensing needle electrodes with alternating polarity between the pulses to reduce electrolytic effects. After flowing through the microchannel (Fig. 3), each 100 μL cell sample is added to 900 μL of LB at room temperature into a 24-well plate and placed in a shaking incubator (250 rpm) at 37 °C for 1 hour recovery. The *E. coli* DH10β and *E. coli* K12 wildtype are diluted by 100 000× or 1000×, respectively prior to selection plating. A total of 100 μL from each sample is plated on ampicillin (50 μg ml^{-1}) containing LB agar plates, and incubated overnight before colony forming units (CFU) quantification.

Positive controls are created by electrotransforming *E. coli* DH10β and *E. coli* K12 wildtype cell suspensions using traditional 2 mm electroporation cuvettes (VWR, Radnor, PA). A total cell suspension volume of 200 μL with 1.0 ng μL^{-1} DNA is pipetted into pre-chilled electroporation cuvettes from the same cell population as the experiments performed in the microchannels. A MicroPulser™ (Bio-Rad, Hercules, CA) is used to pulse the cell suspension at 2.5 kV with about 5 ms time constant. Immediately after delivering the electric pulse, 95 μL of electroporated cells is added to 900 μL of room temperature LB media into a 24-well plate. In order to maintain the number of cells constant with the microchannel experiments, we add an additional 5 μL of cell-DNA mixture into the recovery well and place the plate in a shaking incubator (250 rpm) at 37 °C for 1 hour. Finally, 100 μL of the diluted cell suspension is pipetted onto the ampicillin (50 μg ml^{-1}) containing LB agar plates, and incubated overnight before quantifying CFU using the same dilution ratios as the flow-through experiments.

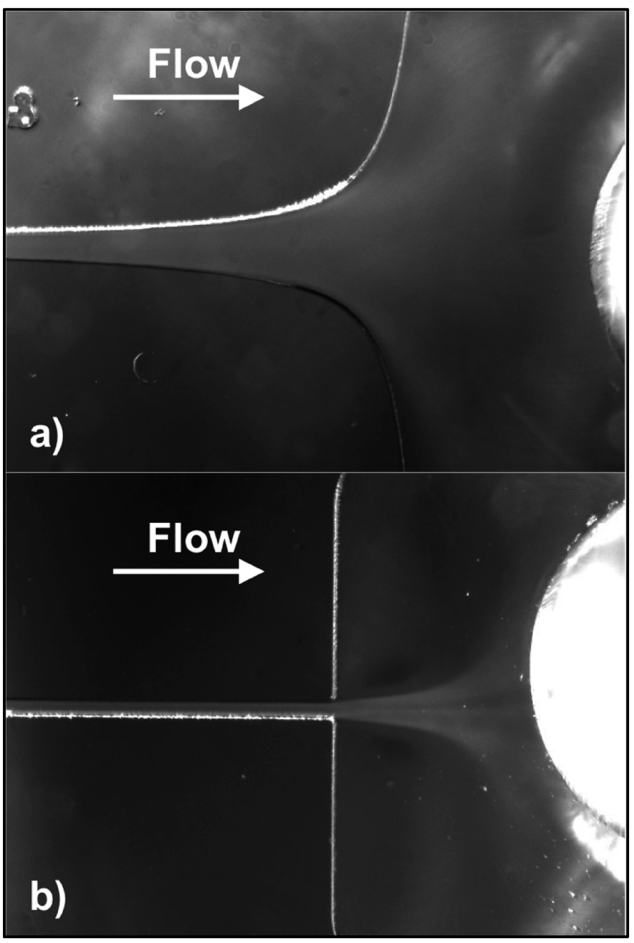

Fig. 3 Microfabricated devices for flow-through bacterial electrotransformation demonstrating the a) bilateral microchannel and the b) straight microchannel geometries with *E. coli* K12 wildtype being electroporated at flow rates of a) 500 μL min^{-1} and b) 125 μL min^{-1}, respectively. Applied voltage 2.5 kV and 5 ms square electroporation pulses with a 95% duty cycle.

Colony forming units quantification for transformation efficiency

After overnight incubation, photos of the agar plates are taken with a Nikon digital camera (Nikon, Tokyo, Japan). Colony forming units (CFUs) are counted by analyzing the photos in the software NICE (NIST's Integrated Colony Enumerator, version 1.2.1) and imageJ (NIH). Here, transformation efficiency is defined as the CFU in ampicillin containing LB agar plates per 1.0 μg DNA.

Statistical methods

One-way ANOVA test is performed to test if transformation efficiency changes significantly with duty cycle of the applied voltage. Student's *t*-test is used for evaluating the effect of channel geometry, flow rate, and applied voltage on transformation efficiency. All statistics are performed on triplicate measurements.

Numerical results and discussion

Channel geometry determines cell specific electric field exposure

Our simulations show that varying the channel geometry results in different time dependent electric field exposure for cells flowing through the microchannels. In particular, the time dependent electric field experienced by cells in a microchannel of non-uniform cross section can be challenging to achieve with standard electronics. Fig. 4 shows the electric field profiles that cells located at the inlet of the constriction will experience due to the flow profile during the 5 ms ON time period during which the square pulse is delivered. In this case, the microchannel geometries from Fig. 3 are identified as bilateral (b) and straight (s) for convenience. As can be seen by the black curves (bilateral geometry), the flow rate influences the exposure time for which cells will experience the electric field. Specifically, a flow rate of 250 μL min^{-1} (black – dotted) exposes the cells to a longer time in an elevated electric field and also requires more time to reach the maximum electric field compared to higher flow rate conditions. Conversely, a flow rate of 1000 μL min^{-1} (black – solid) generates a shorter

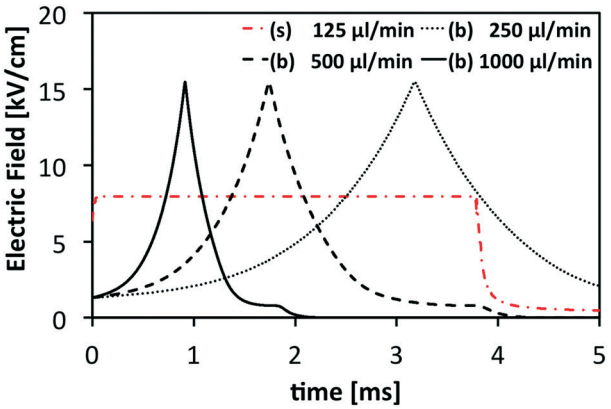

Fig. 4 Time dependent electric field experienced by bacterial cells flowing through the microfluidic device with different microchannel geometries. The channel geometries shown are (s) straight and (b) bilateral as simulated in Fig. 1. The combination of flow rate and channel geometry allow for brief exposure of cells to regions of high electric fields sufficient to induce electroporation and regions of low electric field that may assist in the electrophoretic transfer of nucleic acids into the cells.

exposure of the cells to the high electric field, essentially reducing the 'pulse duration' and reaching the maximum electric field faster. The straight channel geometry (red – dash dot) exposes cells to uniform electric field strength until they exit the constriction. The ability to modulate the exposure duration and specific waveform that the cells experience in a flow-through manner allows for further optimization of electroporation protocols for prokaryotic or eukaryotic cells. Furthermore, continuous and variable electric fields allows for exposure of cells to high electric fields capable of electroporating the cell envelope. Additionally, the device has regions of low electric field to facilitate electrophoretic-assisted transport of DNA into cells.[42]

Minimal joule heating during *E. coli* electrotransformation

As opposed to applications in mammalian cells ($Ø \sim 10$ μm) that require electric fields in the range of 1–2 kV cm^{-1} for successful transfection, bacteria ($Ø \sim 1$ μm) require fields of 10–20 kV cm^{-1} for successful transformation. The use of higher electric fields increases the risk of deleterious Joule heating and compromised cell viability. Therefore, we simulated the Joule heating that is generated during the 5 ms pulse delivery in the bilateral channel with a prescribed flow rate of 500 μl min^{-1} to ensure that cells would not be exposed to lethal temperatures and remain viable (Fig. 5). Fig. 5b shows the temperature distribution at the conclusion of the 5 ms pulse and confirms a localized mild temperature increase ($\Delta T \sim 6$ °C) even after assuming a conservative 5× increase in electrical conductivity during electroporation due to bacterial permeabilization.[43–45] The numerical results demonstrate that this flow rate is able to transport the heated fluid sample outside of the high electric field region within 250 μs after pulse completion (Fig. 5c). We deliver the 5 ms pulses 250 μs after pulse completion to maximize the fraction of electroporated cells. Implementing faster flow rates such as 1000 μL min^{-1}, 2000 μL min^{-1}, and 4000 μL min^{-1} in the bilateral microchannel are non-lethal as well since the cells experience the high electric field for a shorter duration. Therefore, we numerically confirm that a flow-through transformation protocol that requires high electric fields should employ a combination of strong pulsed electric fields, low buffer conductivity, and relatively high flow rates in order to prevent exposing cells to lethal temperatures.[49]

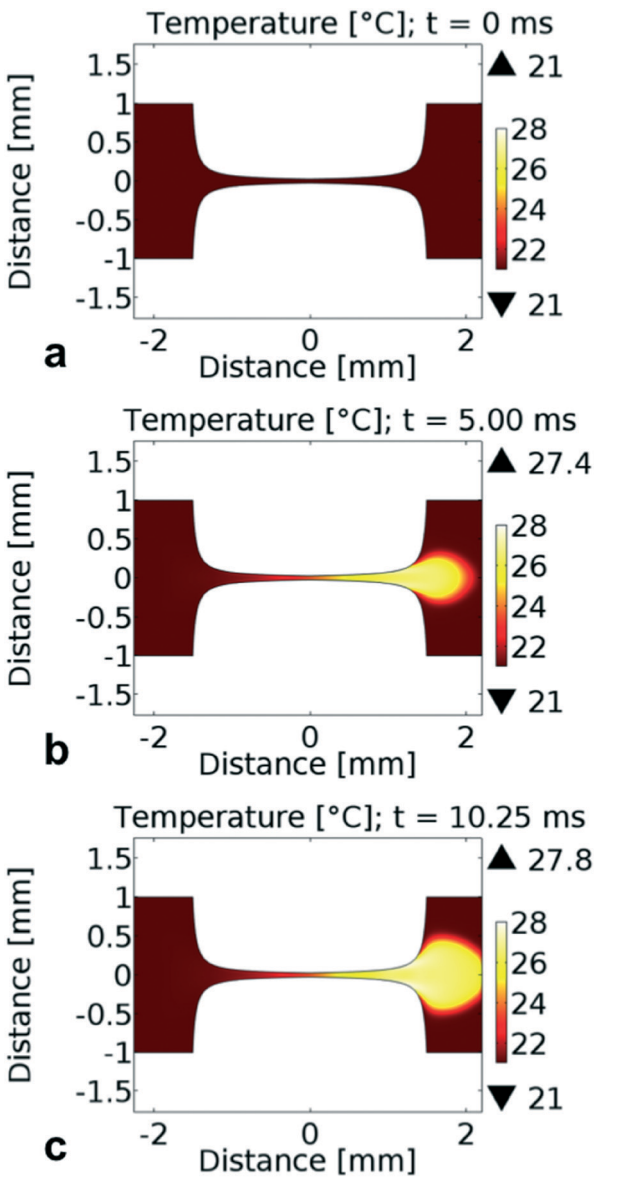

Fig. 5 Simulated temperature distribution in the bilateral microfluidic channel a) before and at the completion of the b) first and c) second pulses. Each square pulse was 5 ms in duration, separated by 250 μs, with applied voltage of 2.5 kV in an experimental sample flowing-through the device at 500 μl min^{-1}.

Experimental results and discussion

Duty cycle evaluation for maximum sample transformation

The duty cycle of the pulses is modulated by defining the OFF time in between the 5 ms square pulses to evaluate the effect of pulse repetition frequency. The goal of characterizing the duty cycle is to maximize the relative amount of transformed sample during flow-through electroporation. Specifically, OFF time durations of 15 ms, 5 ms, and 250 μs between polarity changes correspond to 25%, 50%, and 95% duty cycles, respectively. In all the *E. coli* DH10β samples evaluated, high transformation efficiencies $\geq 6 \times 10^9$ CFU μg^{-1} DNA were achieved with the flow-through techniques using a 500 μL min^{-1} flow rate (Fig. 6). As shown in Fig. 6, one-way ANOVA test gives $p = 0.113$, which suggests a statistically insignificant correlation between transformation efficiency and duty cycle. For all subsequent flow-through electroporation experiments shown in this paper we use a duty cycle of 95% to maximize the percentage of transformed cells.

Flow-through bacterial transformation in microchannels

A single exponentially decaying electric pulse at 2.5 kV with a 5 ms time constant is applied to a 2 mm electroporation cuvette. This is the current experimental standard and is used as a control to determine a base level of electrotransformation. We perform microfluidic electroporation with four different channel designs and use electroporation cuvettes as positive control (Fig. 7). Experimentally, we find that for *E. coli* DH10β and *E. coli* K12 wildtype, electrotransformation with the bilateral microfluidic device is superior to bulk electroporation in cuvettes (Fig. 7). For *E. coli* K12 wildtype, the bilateral microfluidic device shows a statistically significant increase in transformation efficiency, with *p*-values of 0.007, <0.001, 0.010 and 0.002, compared respectively with cuvettes, straight, converging and diverging devices. For *E. coli* DH10β, the *p*-values are 0.070, 0.002, <0.001, and 0.283, when comparing bilateral devices with cuvettes, straight, converging and diverging devices. Even though bilateral devices do not lead to the highest transformation efficiency with DH10β, considering both *E. coli* K12 WT and DH10β data, bilateral devices show the best and most consistent performance in terms of transformation efficiency. Therefore, in subsequent optimization with respect to flow rate and applied voltage, we choose the bilateral microfluidic devices. Our experiments show that in straight microchannels, the least effective geometry tested, the electric field is insufficient to generate transformation efficiencies comparable to the cuvette experiments. These results are consistent with the simulated electric field distributions in which the straight microchannels are unable to amplify the electric fields to the levels achieved with the non-uniform geometries.

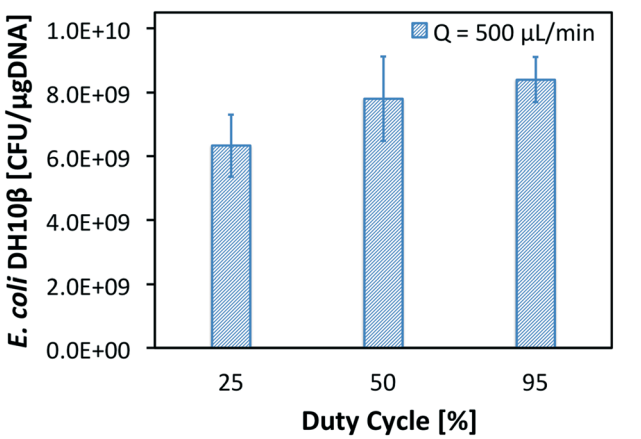

Fig. 6 High efficiency *E. coli* DH10β transformation in the bilateral microfluidic device at 25%, 50%, and 95% duty cycles. Applied voltage = 2.5 kV, 5 ms square electroporation pulses with alternating polarity after each pulse, and 500 μl min^{-1} flow rate were used in the flow-through trials. One-way ANOVA test gives $p = 0.113$, which suggests statistically insignificant correlation between transformation efficiency and duty cycle.

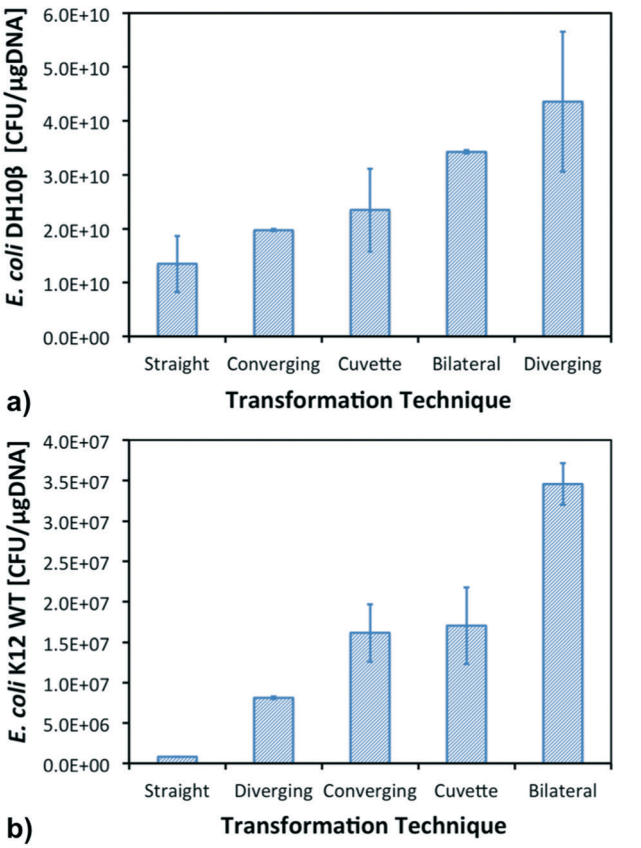

Fig. 7 Transformation efficiency after flow-through electroporation of a) *E. coli* DH10β and b) *E. coli* K12 wildtype in straight (125 μl min^{-1} flow rate) and bilateral (500 μl min^{-1} flow rate) microchannels, 2.5 kV, and 5 ms square electroporation pulses with a 95% duty cycle. Note: flow rates were chosen to ensure that the residence times within the constriction were comparable due to the 4× larger volume between the bilateral and straight constrictions. Note: the positive control in the 2 mm cuvette did not experience any flow.

Effect of volumetric flow rate on bacterial electrotransformation

The volumetric flow rate influences the time dependent electric field experienced by cells in the microchannel geometries. We investigate this phenomenon in the bilateral (Fig. 8a) and straight (Fig. 9a) microchannels. Here, at fixed applied voltage of 2.5 kV, we change the volumetric flow rate from 250–4000 μL min^{-1} in the bilateral microchannel (Fig. 8a) and from 62.5–1000 μL min^{-1} in the straight microchannel (Fig. 9a). When comparing 1000 μL min^{-1} with 250, 500, 2000, and 4000 μL min^{-1} in terms of transformation efficiency in the bilateral microchannel, *t*-test gives *p*-values of 0.016, 0.496, 0.241, and 0.052. Thus, on average, it is shown that a flow rate of 500–2000 μL min^{-1} leads to the highest transformation efficiency in the bilateral channel. Consistent with the 4× difference in constriction volume, the optimal flow rate for the straight geometry was 250–500 μL min^{-1} using the same applied voltage of 2.5 kV (the *p*-values comparing flow of 250 μL min^{-1} with 62.5, 125, 500, 1000 μL min^{-1} are 0.003, 0.044, 0.236, 0.033). These results can be explained by the fact that lower flow rate leads to a longer residence time in the channel and thus prolonged exposure (Fig. 4) to high electric fields or deleterious thermal effects. Conversely, at some point higher flow rates limit the exposure time that the bacteria has at elevated electric fields, reducing the transformation efficiency. It is important to note that the highest average transformation efficiency in the straight microchannel at 250 μL min^{-1} (1.61×10^6 CFU μg^{-1} DNA) was lower than the cuvette electroporation (1.19×10^7 CFU μg^{-1} DNA) shown in Fig. 8a and 9a due to the difference in maximum electric field that can be achieved with each technique.

The ability to achieve comparable or higher transformation efficiencies in our microfluidic devices compared to cuvette electroporation was the initial purpose of this study. However, as the experimental parameter space was evaluated comprehensively, it was discovered that the main advantage of this technique is the potential to significantly increase throughput for certain applications. Fig. 8b demonstrates that using the bilateral channel one can process up to two orders of magnitude more sample volume in a given period of time than using the batch-based cuvettes. This is relevant in applications where continuous transformation is desired such as in the creation of a library of mutants for drug

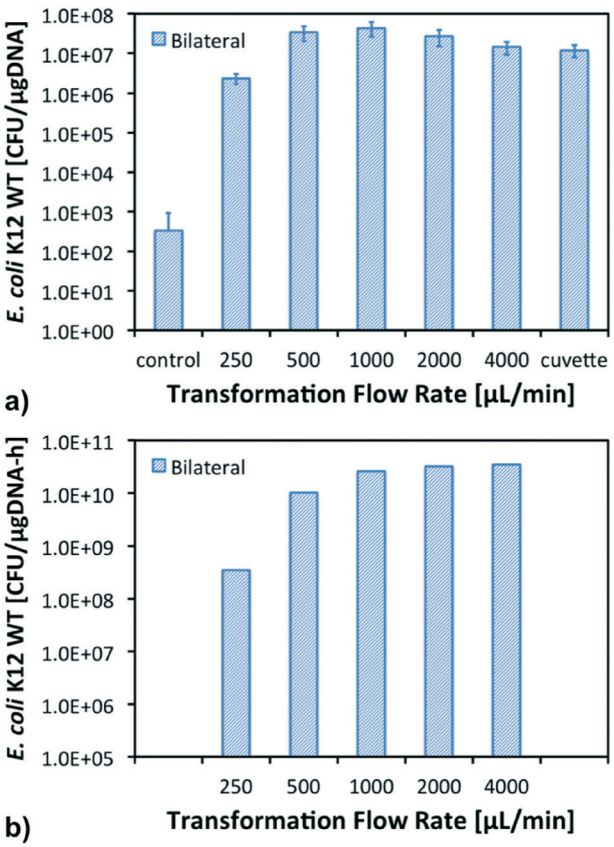

Fig. 8 Transformation efficiency after a) flow-through electroporation of *E. coli* K12 wildtype in bilateral microchannels, 2.5 kV applied, and 5 ms square electroporation pulses with a 95% duty cycle demonstrates an optimal flow rate of 1000 μL min^{-1} for this device. The dramatic increase in throughput can be appreciated in (b) where we quantify the CFU μg^{-1} DNA h^{-1} that can be processed in the bilateral device.

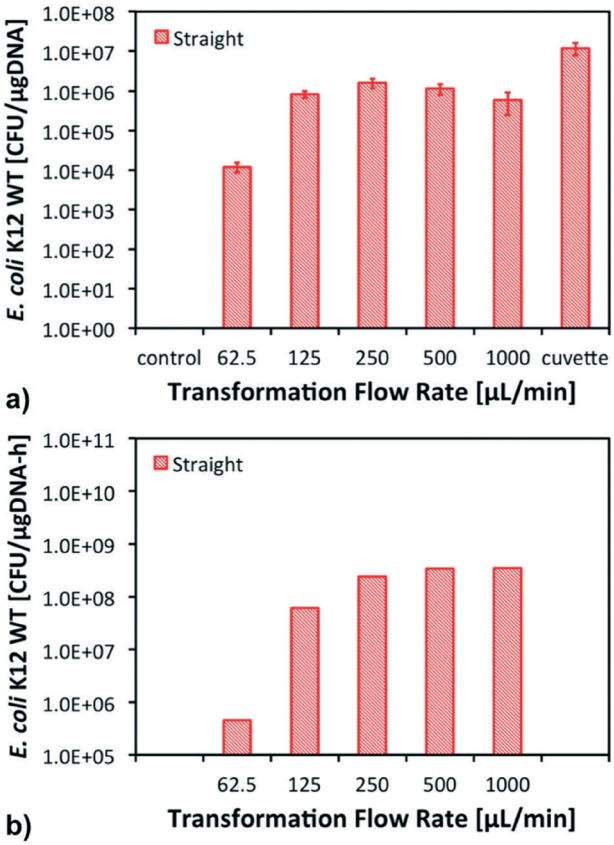

Fig. 9 Transformation efficiency after a) flow-through electroporation of *E. coli* K12 wildtype in straight microchannels, 2.5 kV, and 5 ms square electroporation pulses with a 95% duty cycle. There is increase in throughput b) CFU μg^{-1} DNA h^{-1} that can be processed in the straight device. Note: the highest transformation efficiency achieved at 250 μL min^{-1} (1.61×10^6 CFU μg^{-1} DNA) is still lower than the cuvette electroporation (1.19×10^7 CFU μg^{-1} DNA).

discovery or metabolic engineering.[50–52] Although Fig. 9b shows an increase in the throughput with increasing flow rate in the straight geometry, increasing the electric field is required to achieve comparable CFU μg^{-1} DNA h^{-1} to those achieved in the bilateral channel. The transformation efficiency in straight channels could be improved by increasing the applied voltage and/or reducing the channel width.

Confirmation of flow-through transformation success

Fig. 10 displays the colony forming units (CFU) from electroporated *E. coli* K12 wildtype at an applied voltage of 2.5 kV and with 5 ms square pulses at a 95% duty cycle in the bilateral microchannel. The panels demonstrate the lack of transformed bacteria in the negative control (Fig. 10a) and the baseline transformation in the positive control in cuvettes (Fig. 10f). Fig. 10b–e demonstrate the improved transformation efficiencies with flow rates between 500–2000 $\mu L\ min^{-1}$. These cells were plated in ampicillin containing LB and agar, which was used as a selection method to isolate the successfully transformed bacterial cells.

Effect of applied voltage on flow-through electrotransformation

The influence of applied voltage on the transformation efficiency is tested at a fixed volumetric flow rate of 500 $\mu L\ min^{-1}$ in the bilaterally converging microchannel. The applied voltages are 1.50, 1.75, 2.00, 2.25, and 2.50 kV (Fig. 11). In terms of transformation efficiency, comparing conditions of 2.25 kV with 1.50, 1.75, 2.00 and 2.50 kV, we obtain respectively *p*-values of 0.033, 0.158, 0.407, and 0.820 using *t*-test. Our simulation shows that the peak electric field strength is ~15 kV cm^{-1} when 2.5 kV is applied (Fig. 1a). The increased transformation efficiency can be attributed to the increased electric field strength in the microchannel, which is still below the threshold for killing bacterial cells due to the short exposure time.[53] The transformation efficiency achieved in the bilateral microfluidic device at 1.5 kV is comparable to the transformation efficiency achieved in the straight microchannel at 2.5 kV, demonstrating an additional advantage of the bilateral design.

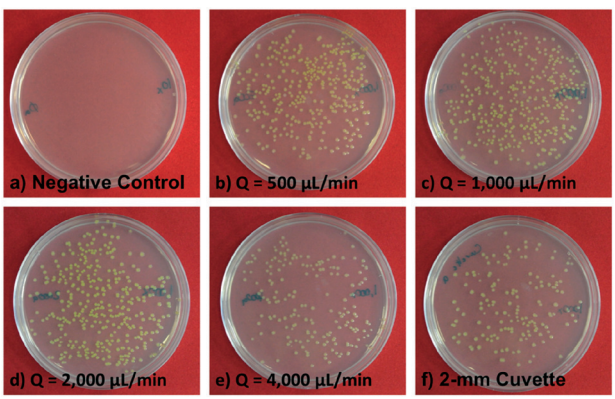

Fig. 10 Colony forming units (CFU) used to quantify transformation efficiencies after flow-through electroporation of *E. coli* K12 wildtype in bilateral microchannels. The experimental parameters involved an applied voltage of 2.5 kV, 5 ms square pulses with a 95% duty cycle, and flow rates of b) 500 $\mu L\ min^{-1}$, c) 1000 $\mu L\ min^{-1}$, d) 2000 $\mu L\ min^{-1}$, and e) 4000 $\mu L\ min^{-1}$ compared to a) negative control or f) cuvette electroporation.

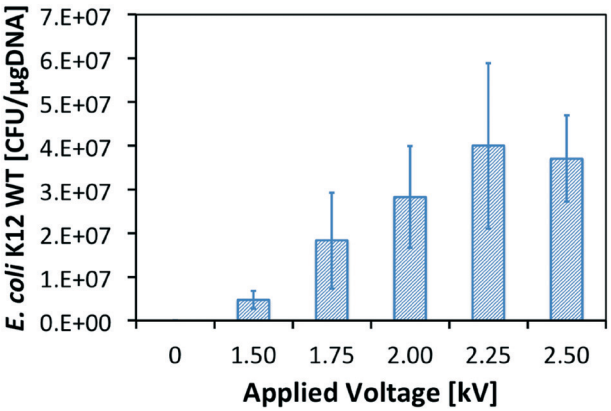

Fig. 11 Transformation efficiency for flow-through electroporation of *E. coli* K12 wildtype in bilateral microchannels. Applied voltages of 1.50, 1.75, 2.00, 2.25, and 2.50 kV with 5 ms square electroporation pulses at a 95% duty cycle were evaluated. The highest average transformation efficiency is observed at an applied voltage of 2.25 kV, which results in E_{max} = 12.5 kV cm^{-1}.

Conclusion

Cell transformation is an essential part of many fields of scientific research including the study of microbial pathogens, metabolic engineering, synthetic biology, and the human microbiome. Improved methods for cell transformation provide researchers a tool to more effectively leverage biology to tackle many of the scientific challenges of our day. Microfluidic flow-through electroporation can be an ideal method for genetic transformation of microbes due to its high transformation efficiency and small sample volume required. While we find that flow-through electroporation can increase transformation efficiency by ~4× for *E. coli* K12 WT when compared to cuvette-based electroporation, we believe this technique's true benefit is the potential to transform up to three orders of magnitude more cells in a given amount of time than in cuvettes.

Further optimization (*e.g.* in channel geometry and flow rate) could potentially increase transformation efficiency for *E. coli* K12 wildtype and other bacterial strains. To our knowledge this work represents the first demonstration of increased bacterial transformation efficiency in a flow-through platform. The combination of increased efficiency and increased throughput compared to traditional cuvette based approaches will result in several orders of magnitude increase in cells transformed in a given amount of time. In future work we will investigate the apparent coupling between transformation efficiency, cumulative electric field exposure, channel geometry, and flow velocity to optimize this process for various bacterial strains. Ultimately the concepts presented

in this paper will yield a flexible transformation platform capable of customization for a wide array of cells, including both prokaryotes and eukaryotes.

Acknowledgements

This work was funded by Defense Advanced Research Projects Agency (DARPA) Living Foundries grant HR0011-15-9-0014, DARPA grant D13AP00025, the NSF CBET 1150615, NSF IIP (I-Corps) 1562925, and NSF IIP (PFI: AIR-TT) 1640678. The authors thank Dr. Jeffrey L. Moran and Dr. Alisha Schor for insightful scientific conversations. We also thank Kurt Broderick and the MIT Microsystems Technology Laboratory (MTL) for microfabrication training and N. R. Fuller from Sayo-Art, LLC for schematic artwork in Fig. 2.

References

1 M. Mimee, R. J. Citorik and T. K. Lu, *Adv. Drug Delivery Rev.*, 2016, **105**(Part A), 44–54.
2 C. Liu, B. C. Colón, M. Ziesack, P. A. Silver and D. G. Nocera, *Science*, 2016, **352**, 1210–1213.
3 K. Pardee, S. Slomovic, P. Q. Nguyen, J. W. Lee, N. Donghia, D. Burrill, T. Ferrante, F. R. McSorley, Y. Furuta, A. Vernet, M. Lewandowski, C. N. Boddy, N. S. Joshi and J. J. Collins, *Cell*, 2016, **167**(1), 248–259.e12.
4 S. Slomovic, K. Pardee and J. J. Collins, *Proc. Natl. Acad. Sci. U. S. A.*, 2015, **112**, 14429–14435.
5 M. O. Din, T. Danino, A. Prindle, M. Skalak, J. Selimkhanov, K. Allen, E. Julio, E. Atolia, L. S. Tsimring, S. N. Bhatia and J. Hasty, *Nature*, 2016, **536**, 81–85.
6 H. Ando, S. Lemire, D. P. Pires and T. K. Lu, *Cell Syst*, 2015, **1**, 187–196.
7 A. D. Miller and G. J. Rosman, *BioTechniques*, 1989, **7**, 980.
8 C. E. Thomas, A. Ehrhardt and M. A. Kay, *Nat Rev Genet*, 2003, **4**, 346–358.
9 E. L. Wollman, F. Jacob and W. Hayes, *Cold Spring Harbor Symp. Quant. Biol.*, 1956, **21**, 141–162.
10 P. Trieucuot, C. Carlier, P. Martin and P. Courvalin, *Fems Microbiol Lett*, 1987, **48**, 289–294.
11 C. M. Thomas and K. M. Nielsen, *Nat. Rev. Microbiol.*, 2005, **3**, 711–721.
12 A. Adamo, A. Arione, A. Sharei and K. F. Jensen, *Anal. Chem.*, 2013, **85**, 1637–1641.
13 A. Sharei, J. Zoldan, A. Adamo, W. Y. Sim, N. Cho, E. Jackson, S. Mao, S. Schneider, M. J. Han, A. Lytton-Jean, P. A. Basto, S. Jhunjhunwala, J. Lee, D. A. Heller, J. W. Kang, G. C. Hartoularos, K. S. Kim, D. G. Anderson, R. Langer and K. F. Jensen, *Proc. Natl. Acad. Sci. U. S. A.*, 2013, **110**, 2082–2087.
14 E. Neumann, M. Schaefer-Ridder, Y. Wang and P. H. Hofschneider, *J. EMBO*, 1982, **1**, 841–845.
15 *Guide to Electroporation and Electrofusion*, ed. D. C. Chang, B. M. Chassy, J. A. Saunders and A. E. Sowers, Academic Press, 1991.
16 Y. Sheng, V. Mancino and B. Birren, *Nucleic Acids Res.*, 1995, **23**, 1990–1996.
17 M. L. Yarmush, A. Golberg, G. Serša, T. Kotnik and D. Miklavčič, *Annu. Rev. Biomed. Eng.*, 2014, **16**, 295–320.
18 T. Kotnik, W. Frey, M. Sack, S. Haberl Meglic, M. Peterka and D. Miklavcic, *Trends in biotechnology*, 2015, DOI: 10.1016/j.tibtech.2015.06.002.
19 H. Y. Wang, A. K. Bhunia and C. Lu, *Biosens. Bioelectron.*, 2006, **22**, 582–588.
20 R. V. Davalos, L. M. Mir and B. Rubinsky, *Ann. Biomed. Eng.*, 2005, **33**, 223–231.
21 J. H. Rossmeisl, P. A. Garcia, T. E. Pancotto, J. L. Robertson, N. Henao-Guerrero, R. E. Neal II, T. L. Ellis and R. V. Davalos, *J. Neurosurg.*, 2015, 1–18.
22 R. C. Martin 2nd, K. McFarland, S. Ellis and V. Velanovich, *Ann. Surg. Oncol.*, 2012, DOI: 10.1245/s10434-012-2736-1.
23 R. Cannon, S. Ellis, D. Hayes, G. Narayanan and R. C. Martin 2nd, *J. Surg. Oncol.*, 2013, **107**, 544–549.
24 D. Miklavcic, D. Semrov, H. Mekid and L. M. Mir, *Biochim. Biophys. Acta*, 2000, **1523**, 73–83.
25 T. Kotnik, G. Pucihar, M. Rebersek, D. Miklavcic and L. M. Mir, *Biochim. Biophys. Acta, Biomembr.*, 2003, **1614**, 193–200.
26 P. A. Garcia, Z. Ge, J. L. Moran and C. R. Buie, *Sci. Rep.*, 2016, **6**, 21238.
27 T. Geng and C. Lu, *Lab Chip*, 2013, **13**, 3803–3821.
28 W. G. Lee, U. Demirci and A. Khademhosseini, *Integr. Biol.*, 2009, **1**, 242–251.
29 S. Wang and L. J. Lee, *Biomicrofluidics*, 2013, **7**, 011301.
30 Y. Huang and B. Rubinsky, *Sens. Actuators, A*, 2003, **104**, 205–212.
31 L. Chang, P. Bertani, D. Gallego-Perez, Z. Yang, F. Chen, C. Chiang, V. Malkoc, T. Kuang, K. Gao, L. J. Lee and W. Lu, *Nanoscale*, 2016, **8**, 243–252.
32 Z. G. Yang, L. Q. Chang, C. L. Chiang and L. J. Lee, *Curr. Pharm. Des.*, 2015, **21**, 6081–6088.
33 L. Q. Chang, D. Gallego-Perez, X. Zhao, P. Bertani, Z. G. Yang, C. L. Chiang, V. Malkoc, J. F. Shi, C. K. Sen, L. Odonnell, J. H. Yu, W. Lu and L. J. Lee, *Lab Chip*, 2015, **15**, 3147–3153.
34 L. Q. Chang, M. Howdyshell, W. C. Liao, C. L. Chiang, D. Gallego-Perez, Z. G. Yang, W. Lu, J. C. Byrd, N. Muthusamy, L. J. Lee and R. Sooryakumar, *Small*, 2015, **11**, 1818–1828.
35 M. Khine, A. Lau, C. Ionescu-Zanetti, J. Seo and L. P. Lee, *Lab Chip*, 2005, **5**, 38–43.
36 P. E. Boukany, A. Morss, W.-C. Liao, B. Henslee, H. Jung, X. Zhang, B. Yu, X. Wang, Y. Wu, L. Li, K. Gao, X. Hu, X. Zhao, O. Hemminger, W. Lu, G. P. Lafyatis and L. J. Lee, *Nat. Nanotechnol.*, 2011, **6**, 747–754.
37 W. Kang, J. P. Giraldo-Vela, S. S. P. Nathamgari, T. McGuire, R. L. McNaughton, J. A. Kessler and H. D. Espinosa, *Lab Chip*, 2014, **14**, 4486–4495.
38 T. Geng, Y. Zhan, J. Wang and C. Lu, *Nat. Protoc.*, 2011, **6**, 1192–1208.
39 Y. H. Zhan, Z. N. Cao, N. Bao, J. B. Li, J. Wang, T. Geng, H. Lin and C. Lu, *J. Controlled Release*, 2012, **160**, 570–576.

40 J. Wang, Y. Zhan, V. M. Ugaz and C. Lu, *Lab Chip*, 2010, **10**, 2057–2061.
41 H. Yun and S. C. Hur, *Lab Chip*, 2013, **13**, 2764–2772.
42 J. M. Escoffre, T. Portet, L. Wasungu, J. Teissie, D. Dean and M. P. Rols, *Mol. Biotechnol.*, 2009, **41**, 286–295.
43 A. Silve, I. Leray, C. Poignard and L. M. Mir, *Sci. Rep.*, 2016, **6**, 19957.
44 D. Sel, D. Cukjati, D. Batiuskaite, T. Slivnik, L. M. Mir and D. Miklavcic, *IEEE Trans. Biomed. Eng.*, 2005, **52**, 816–827.
45 P. A. Garcia, J. H. Rossmeisl, R. E. Neal II, T. L. Ellis, J. Olson, N. Henao-Guerrero, J. Robertson and R. V. Davalos, *J. Membr. Biol.*, 2010, **236**, 127–136.
46 B. del Rosal, C. Sun, D. N. Loufakis, C. Lu and D. Jaque, *Lab Chip*, 2013, **13**, 3119–3127.
47 R. C. Gallo-Villanueva, M. B. Sano, B. H. Lapizco-Encinas and R. V. Davalos, *Electrophoresis*, 2014, **35**, 352–361.
48 S. E. Luria and M. L. Human, *J. Bacteriol.*, 1952, **64**, 557–569.
49 P. A. Garcia, R. V. Davalos and D. Miklavcic, *PLoS One*, 2014, **9**, e103083.
50 M. J. Smanski, S. Bhatia, D. Zhao, Y. Park, L. B. A. Woodruff, G. Giannoukos, D. Ciulla, M. Busby, J. Calderon, R. Nicol, D. B. Gordon, D. Densmore and C. A. Voigt, *Nat. Biotechnol*, 2014, **32**, 1241–1249.
51 D. M. Fowler and S. Fields, *Nat Meth*, 2014, **11**, 801–807.
52 C. D. Aakre, J. Herrou, T. N. Phung, B. S. Perchuk, S. Crosson and M. T. Laub, *Cell*, 2015, **163**, 594–606.
53 I. Álvarez, R. Virto, J. Raso and S. Condón, *Innovative Food Sci. Emerging Technol.*, 2003, **4**, 195–202.
54 M. E. Pyne, M. Moo-Young, D. A. Chung and C. P. Chou, *Biotechnol. Biofuels*, 2013, **6**, 50.